UR-NCUR 11-28

THE UNIVERSITY OF ROCHESTER

Nuclear Science Research Group

ROCHESTER, NEW YORK 14267-0216, USA

Isoscaling in projectile breakup following dissipative $^{48}Ca+^{112}Sn$ and $^{48}Ca+^{124}Sn$ reactions at E/A=45 MeV

ISOCHIM Collaboration: H. Singh, M. J. Quinlan, J. Tõke, I. Pawelczak, E. Henry, W. U. Schröder, F. Amorini, A. Anzalone, C. Maiolino, L. Auditore, D. Loria, A. Trifiro, M. Trimarchı, G. Cardella, E. De Filippo, A. Pagano, M.B. Chatterjee, S. Cavallaro, E. Geraci, M. Papa, S. Pirrone, G. Verde, A. Grzeszczuk, P. Guazzoni, L. Zetta, E. La Guidara, G. Lanzalone, S. Lo Nigro, G. Politi, D. Loria, F. Porto, F. Rizzo, P. Russotto, M. Vigilante

Draft: November 2011

Isoscaling in projectile breakup following dissipative $^{48}Ca+^{112}Sn$ and $^{48}Ca+^{124}Sn$ reactions at E/A=45 MeV

H. Singh[1], M. J. Quinlan[1], J. Tõke[1], I. Pawelczak[1], E. Henry[1], W. U. Schröder[1], F. Amorini[2], A. Anzalone[2], C. Maiolino[2], L. Auditore[3], D. Loria[3], A. Trifiro[3], M. Trimarchı[3], G. Cardella[4], E. De Filippo[4], A. Pagano[4], M.B. Chatterjee[5], S. Cavallaro[4,6], E. Geraci[4,6], M. Papa[4], S. Pirrone[4], G. Verde[4], A. Grzeszczuk[7], P. Guazzoni[8], L. Zetta[8], E. La Guidara[4,9], G. Lanzalone[10], S. Lo Nigro[6], G. Politi[4,6], D. Loria[11], F. Porto[2,6], F. Rizzo[2,6], P. Russotto[2,6], M. Vigilante[13]

[1]*Departments of Chemistry and Physics, University of Rochester, Rochester NY, USA*
[2]*INFN Laboratori Nazionali del Sud, Catania, Italy*
[3]*INFN Gruppo coll. Di Messina & Dipartimento di Fisica Universita di Messina, Messina, Italy*
[4]*INFN Sezione di Catania, Italy*
[5]*Saha Institute for Nuclear Physics, Kolkata, India*
[6] *Dipartimento di Fisica e Astronomia, Universitıa di Catania, Italy*
[7]*Institute of Physics, University of Silesia, Katowice, Poland*
[8]*INFN Sezione di Milano & Dipartimento di Fisica Universita di Milano, Italy*
[9] *CSFNSM, Catania, Italy*
[10]*INFN Laboratori Nazionali del Sud, Catania, & Universita KORE Enna, Italy*
[11]*INFN Gruppo coll. Di Messina & Dipartimento di Fisica, Universita di Messina, Italy*
[12]*INFN Sezione di Napoli & Dipartimento di Fisica Universi´a Federico II di Napoli, Napoli, Italy*

ABSTRACT

Results are presented for the distributions of products generated in the dynamical breakup of projectile-like fragments (PLF) following dissipative reactions of ^{48}Ca projectiles with ^{112}Sn and ^{124}Sn target nuclei. Aligned breakup kinematics and fragment yields suggest that PLF splitting occurs in the proximity of the target-like fragment (TLF) under the influence of nuclear interactions. The isotopic distributions of intermediate-mass clusters with Z = 3-7 from PLF breakup exhibit "isoscaling" regularities that can be understood in terms of a simple phase space model governed by ground state mass differences. However, the derived isoscaling parameters show ambiguities, whose resolution requires knowledge of the primary reaction scenario. This requirement further complicates attempts to derive the nuclear symmetry energy at subnormal densities. Theoretical molecular-dynamics and one-body transport simulation calculations fail to reproduce experimental data.

I. INTRODUCTION

The present article reports on results obtained by the CECIL collaboration at the Laboratori Nazionali del Sud (LNS) Catania in a study of multi-particle correlations in the reactions $^{48}Ca+^{112}Sn$ and $^{48}Ca+^{124}Sn$ at an "intermediate" laboratory bombarding energy of E/A = 45 MeV. Intermediate-energy heavy-ion reactions mark the interesting transition from a mean-field (one-body) dominated mass and energy flow between interacting nuclei to the domain of viscous nuclear hydrodynamics. Such heavy-ion reactions can presumably also produce excited nuclear systems at the limits of mechanical and chemical stability [1-3], with unusual mass density profiles [4] and decay patterns [5] not observed in other processes [6].

A major objective of the present experiment was to explore regularities in the isotopic distributions of products emitted following dissipative interactions [7] of the same projectile (^{48}Ca) with target nuclei of different A/Z ratios. Such different entrance channel A/Z or "isospin" asymmetries are expected [7] to generate isospin dependent driving potentials affecting the differential exchanges of neutrons and protons between projectile and target nuclei which in the process may acquire substantial excitations and diluted matter distributions.

In principle, intermediate-energy heavy-ion reactions may provide access to the equilibrium nuclear equation of state (EOS) [8], specifically to the density dependence of the nuclear symmetry energy [9]. This type of information is not only of interest to basic nuclear science. It is also needed to understand cosmological phenomena, both structures and processes. An essential prerequisite for a valid interpretation of reaction data is a realistic assessment of pre-equilibrium effects [10, 11] and an understanding of the degree of equilibration reached by the systems under study. Earlier works [12, 13] have demonstrated that fast pre-equilibrium particle emission does not only limit the energy available for nuclear excitation but can significantly and unpredictably alter the identities of these systems in Z and A. To be able to disentangle even some of these complexities puts high demands on the experimental event coverage, favoring 4π particle detection such as afforded by the CHIMERA multi-detector array [14-16] at LNS Catania.

Unfortunately, regularities in the isotopic distributions of observed light particles, intermediate-mass or more massive fragments arises from a combination of

effects associated with primary reaction and secondary decay. Obviously, the main interest concerns the former regularities, those exhibited by the primary reaction products, which poses the problem as to how to unravel the desired information on the effective symmetry energy hidden in the observations. This task certainly requires a comprehensive evaluation of the various exit channel components, including particles produced in fast emission and slower fission-like and evaporation processes.

The following section presents a brief summary of experimental and analytical procedures. Section III presents experimental evidence for the reaction mechanisms leading to the emission of intermediate-mass cluster fragments. The observed isotopic regularities are discussed and interpreted in Section IV.

II. EXPERIMENTAL PROCEDURES

The experiment was carried out using the K800 cyclotron at the LNS Catania. Isotopically enriched, self-supporting targets of ^{124}Sn and ^{112}Sn with thicknesses of 689 μg/cm2 and 627 μg/cm^2, respectively, were placed inside the CHIMERA array. The targets were bombarded with a pulsed ^{48}Ca beam of energy E/A = 45 MeV. The beam had a repetition period of 120 ns. The CHIMERA array consists of 1192 ΔE-E (Si-CsI(Tl)) telescopes which cover ~94% of the solid angle. Each telescope consists of a 300-μm thick silicon detector, while CsI(Tl) detectors have different thicknesses depending on the polar angle θ.

Energy calibrations for silicon detectors were carried out using ^{12}C and ^{16}O beams from the LNS MP Tandem accelerator, along with elastically scattered ^{48}Ca projectiles. Except for several test and calibration runs, the data acquisition system was set to trigger on a minimum-bias

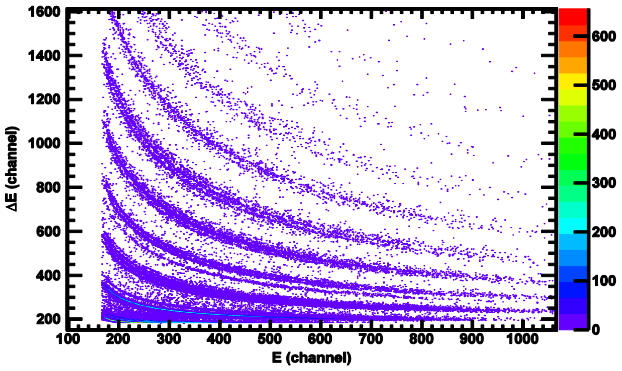

Figure 1: Raw event correlation between energy deposit in the Si detector and total energy measured for the ^{48}Ca + ^{124}Sn reaction at a laboratory angle of θ = 19^o. The cutoff at channel number 165 is due to electronic thresholds.

condition of charged-particle multiplicity M ≥ 2, thus excluding elastic scattering and weakly dissipative collisions from being recorded. Reaction products were characterized according to atomic number Z, mass number A, energy and emission angles, utilizing the measured time of flight (TOF), energy and light output information obtained from the ΔE-E telescopes. More details on the experimental setup are provided elsewhere [Quinlan, 2011 PhD].

For the present study, mostly data collected in the forward angular region ($6^o \leq \theta \leq 20^o$) were considered. These data comprise the fast, projectile-like fragments (PLF), as well as their decay products. Care was taken to exclude from the present consideration any product associated with the decay of the target-like fragment (TLF).

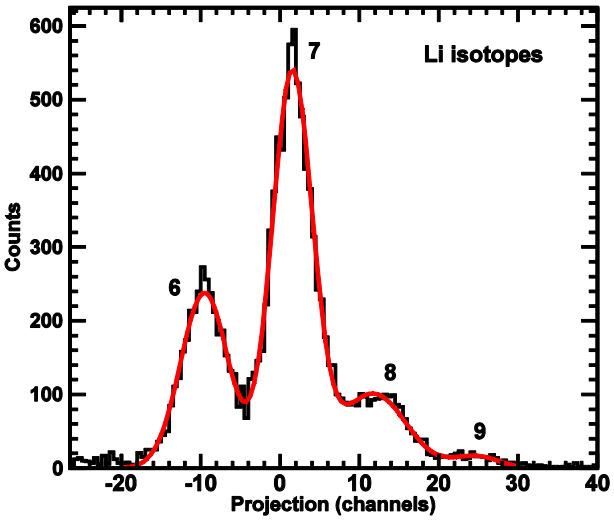

Figure 2: Histogram of the angle integrated isotopic distribution for Li fragments from the ^{48}Ca + ^{124}Sn reaction. The curve represents a Gaussian fit.

As an example for raw data obtained for light charged particles (LCP) and intermediate-mass fragments (IMF), a 2-dimensional correlation plot is given in Fig. 1, demonstrating isotopic separation for elements with 1 ≤ Z ≤ 9. Fig. 2 provides a linearized plot of angle-integrated data for Li-isotopes emitted in the reaction ^{48}Ca + ^{124}Sn. The smooth line drawn through the data represents a multiple Gaussian fit to the sum yield for 6≤ A ≤9. A good isotopic resolution of the detection system is clearly visible in this figure. It also shows the production probability to be at a maximum for the β-stable isotope ^{7}Li.

The good angular coverage afforded by the CHIMERA array allowed a reasonably realistic reconstruction of the event history to be performed from correlated particle emission patterns. For example, Ca-like PLF fragments were reconstructed kinematically from the fast, forward emitted ensemble of PLF remnants, IMFs and LCPs. In such events, much of the reconstructed mass and charge was observed in form of pairs of one correlated IMF (3 ≤ Z ≤ 5) and a corresponding heavier PLF remnant. Further details of measurement and analysis are reported elsewhere [17].

In order to obtain an overview overall of the reactive scenario, the following discussion will concentrate on the behavior of the reconstructed PLF (IMF+PLF remnant) and the modalities of its disintegration, as evidenced in the observed fragment emission patterns.

III. Reaction Mechanism: Dynamic Projectile Breakup Following Dissipative Collisions

As discussed above, in the present experiment a reconstruction of the event reaction history prior to the subsequent fragment disintegration has approximately been possible for the present ^{48}Ca+^{112}Sn and ^{48}Ca+^{124}Sn reactions at E/A=45 MeV.

Interesting results are illustrated in Fig. 3 for the reaction ^{48}Ca+^{112}Sn. Here, Wilczyński-type contour diagrams of the yield are shown on logarithmic scale, for the reconstructed PLF kinetic energy (T_PLF, top) and the PLF velocity (|v|_PLF, bottom). On average, the experimental yield ridges appear to evolve with PLF laboratory angle and kinetic energy as expected (solid dots and curve in upper panel) for a dissipative reaction. The open symbols connected by a curve in Fig. 3a represent calculations with dissipative reaction code CLAT [18]. The solid

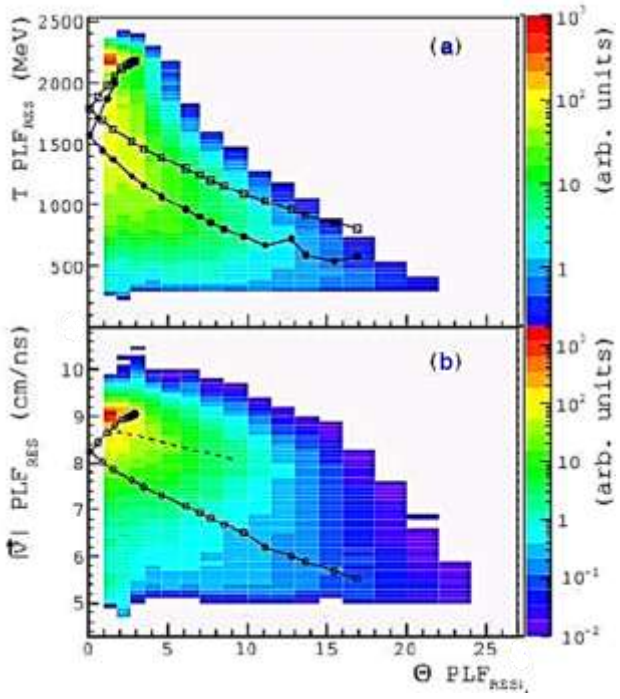

Figure 3: Experimental Wilczyński contour diagrams for the reaction ^{48}Ca+^{124}Sn @E/A=45 MeV. Top: PLF energy vs. angle, bottom: PLF velocity vs. angle. Symbols and curves represent mean predictions by the nucleon exchange model (CLAT).Sequential evaporation is accounted for using the GEMINI code. The dashed curve (in b) guides the eye along the evolution of the main yield with angle.

symbols represent the same calculations but corrected for sequential nuclear decay using the code GEMINI [19].

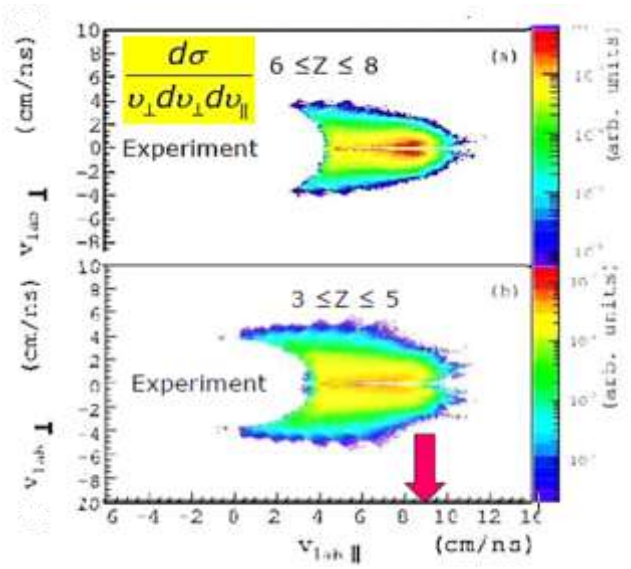

Figure 4: Galilei invariant cross section contour diagrams, plotted vs. parallel and perpendicular velocities, for heavier PLF remnants (a) and IMFs (b). The arrow indicates the beam velocity. The semi-circular boundary at low parallel velocities indicates detection thresholds.

However, it turns out that the agreement between theory and data illustrated in Fig. 3a is deceptive. As demonstrated by Fig. 3b showing the same data as in Fig 3a, but now plotted vs. mean PLF velocity instead of PLF kinetic energy, significant discrepancies between theory and data do exist. Less kinetic energy than predicted appears to be dissipated in the reaction. Such discrepancy with data is not limited to the particular model illustrated in Fig. 3. Similar, if not larger, discrepancies are found in corresponding comparisons between data and more microscopic QMD calculations [20].

The above apparent inconsistency of experimental Wilczyński-type diagrams plotted vs. different observables is resolved by the observation that the PLF, after its dissipative interaction with the target-like nucleus (TLF), does not decay in a statistical fashion. Rather, the excited PLF appears to break up in a fashion dominated by dynamical effects, which may be generated by the proximity of the TLF. This conclusion is suggested by data for the same reaction ^{48}Ca+^{112}Sn such as shown, in Fig. 4a for the heavier and in Fig. 4b for the lighter, intermediate-mass (IMF) PLF remnants, respectively. In this figure, logarithmic contours of the respective Galilei invariant cross sections $d^2\sigma/\left(\upsilon_\perp d\upsilon_\perp d\upsilon_\parallel\right)$ are plotted vs. velocity components parallel and perpendicular to the beam direction. PLF remnants are selected at forward angles ($|Q_{PLF}|<18^0$), which are kinematically inaccessible by such particles if emitted from the TLF. The elongated emission patterns observed in Fig. 4 are obviously very different from the circular patterns expected for sequential statistical emission from a PLF source disintegrating in flight.

In fact, there are several additional pieces of experimental evidence supporting a mechanism in which the PLF, after its dissipative interaction with the target-like nucleus (TLF), breaks up or splits in a fashion dominated by dynamics. As discussed in detail elsewhere [17] the

list of such supporting pieces of evidence includes the following observations:

1. The PLF breakup/split axis lies predominantly in the reaction plane.
2. The orientation of the breakup axis is aligned with the direction of flight of the reconstructed PLF.
3. The relative velocities of the breakup fragments are significantly larger than those given by Coulomb repulsion and largest in forward and backward directions.
4. For asymmetric PLF splits, the smaller PLF remnant is preferentially emitted in the backward direction (towards the TLF) with exponentially enhanced yields.
5. Finally, there is a noticeable component of symmetric PLF splits that, according to the Businaro-Gallone criterion, is not expected for equilibrium statistical decay of a light, Ca-like PLF.

Inelastic, dynamical breakup is a well-known process in the Fermi energy domain [21, 22] for reactions induced by lighter projectiles, most often by projectiles exhibiting

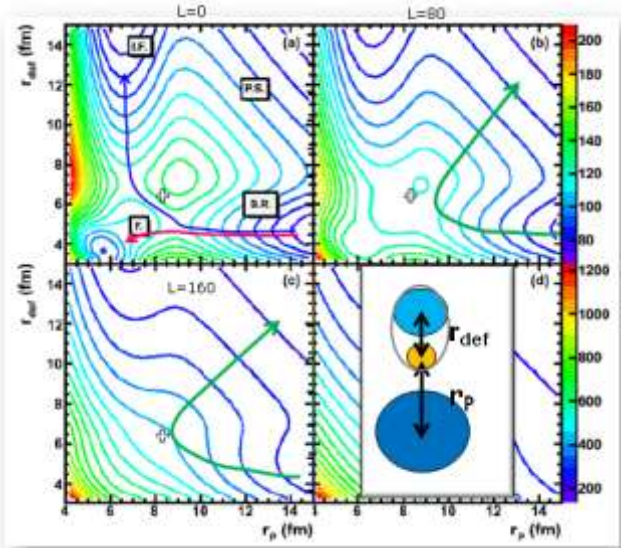

Figure 5: 3-body potential energy surface (PES) and schematic trajectories for PLF breakup in the field of the TLF for angular momenta L=0, 80 and 160. The PES is plotted vs. PLF deformation parameter r_{def} and PLF-TLF distance, r_p. The deformed configuration assumed for the PLF is depicted in panel (d).

cluster structure. Naturally, instability induced by such structure promotes massive-cluster transfer between projectile and target or incomplete fusion, which has also been observed in this energy domain. Here the projectile attains a highly deformed, near-breakup configuration in the approach phase when overlapping with the target nucleus, before receding again in the exit channel. Figure 5 presents a contour diagram of relevant three-body potential energy surfaces (PES), calculated from Coulomb, proximity nuclear and centrifugal potentials, for various relative angular momenta L. As schematically indicated in Fig. 5d, for the purpose of generating a PES, the projectile configuration is approximated by a pair of fragments, separated as given by a deformation parameter r_{def}, and at a distance r_p from the target-like nucleus. Note, that in all PES diagrams shown in Fig. 5, the lighter of the two PLF fragments is oriented towards the target-like reaction partner. Also shown in this figure are schematic system trajectories illustrating the competition between different reaction modes.

The L=0 PES (Fig. 5 a) displays the interesting topology featuring a deep potential pocket that could lead to complete fusion (F), as well as features driving the system to incomplete fusion (IF) or PLF splitting (P.S.) without capture of any of the PLF remnants. The binary reaction entrance channel is denoted as B.R. in Fig. 5a.

For intermediate L waves (Fig. 5b), i.e., more peripheral interactions, complete and incomplete fusion minima or depressions become shallower and eventually disappear from the PES. Here, an apparent PES gradient (P.S.) drives an excited PLF to sequential splitting in the proximity and under the influence of the TLF. For a reverse orientation of the PLF breakup fragments, where the heavier part faces the TLF, the PES has a generally less structured topology. Incomplete fusion of the TLF with a heavy PLF portion is less likely than for a lighter component, a plausible scenario.

The process illustrated above resembles dynamic ternary fission, a process that has been discussed in the literature since many years [23-25]. Various theoretical approaches consider the ejection of an alpha particle or small nuclear clusters in the collapse of a matter bridge ("neck") formed between two main fragments. The probability Y for the ejection of such cluster from an initially contiguous surface to a region between the nuclear surfaces of the nascent main fragments and the overall Coulomb barrier has been calculated [24] as

$$P \propto \left(\frac{T^{5/2}}{F_s} \right) \cdot \exp\{ -\frac{\Delta E_s}{T_{eff}} \} \qquad (1)$$

Here, ΔE_s is the energy required for the particles to cross the surface, T_{eff} is an effective nuclear temperature, and F_s is the force acting on the particle in that transition. In such a picture, the main dependence of the particle yields have the same form as in statistical phase space models [23, 25], where third-particle yields are modeled in a fashion similar to Boltzmann statistics,

$$P \propto \exp\{ \frac{(Q - V_{Coul})}{T} \} \qquad (2)$$

In Equ. 2, the energy exponent contains the Q value for formation, the Coulomb barrier V_{Coul} for emission of the particle and the specific thermal energy T. While in the latter models this energy is assumed to be equal to the equilibrium system temperature T, in non-equilibrium theories of particle emission in nuclear reactions, this quantity is identified with the energy $T_{eff} > T$ available for the excitation of a subset of all possible system configurations relevant for the specific process. As an example, pre-equilibrium theories of nuclear decay [10, 11] consider the energy transferred to an initial set of particle-hole pairs (excitons) in a struck nucleus to be the dominant condition for its non-statistical disintegration. In all plausible phase space model scenarios, it is the potential increase in entropy S or in the associated number of accessed configurations, $\varpi \propto \exp\{S\}$, which drives the time

dependent process and determines the cluster yields in ternary fission. This conclusion also applies for the dynamical breakup process considered here, adding a layer of ambiguity to the interpretation of experimental cluster yields.

To produce supporting evidence for the viability of a speculative picture such as outlined above requires realistic 3-body reaction simulations that take into account dissipation and associated changes in the interactions of hot and expanded nuclei. Such simulations are being considered but are not yet available anywhere. Nor can one expect popular QMD or BUU models to be capable of addressing the observed multi-particle correlations. This conclusion is illustrated by the experience made in the present case with QMD calculations (cf. Sect. III). These models incorporate different approximations of a mean field and residual 2-body nucleon-nucleon interactions.

IV. ISOSCALING IN PLF BREAKUP

A. GENERAL CONSIDERATIONS

As pointed out previously, major motivation for a study of dissipative heavy-ion reactions at intermediate bombarding energies derives from the hope to thereby assess independently the symmetry energy of nuclear systems at diluted mass densities. Nuclei with subnormal mass densities are expected to result from thermal expansion of very hot, but still meta-stable primary reaction products, e.g., the PLFs and/or TLFs emerging from dissipative reactions or the composite nuclei produced in nuclear fusion. The term *meta-stable* is employed here in the usual, pragmatic sense allowing one to apply equilibrium thermodynamics to an unstable nuclear system.

In a statistical disintegration or decay of meta-stable primary products, final daughter fragments are expected with yields reflecting the multiplicity of partitions of the available energy among the possible populations of configuration and phase space. Since heavier nuclear clusters can be emitted only from hot, diluted nuclear systems, likely from their surfaces, cluster isotopic distributions are expected to reflect the mean-field symmetry energy for such systems. On the other hand, nucleons and very light charged particles, which are also subject to mean-field interactions, can be emitted already from the initial cold system and then at different stages of the reaction characterized by various degrees of energy dissipation, relaxation and nuclear expansion. In addition, nucleon emission undergoes in-medium scattering, mixing the effects of mean field and residual interactions in the isospin dependent signals these particles also carry. Therefore, isotopic effects in nuclear cluster emission should reflect the underlying symmetry energy more directly than light-particle processes.

Assumptions of meta-stable equilibrium and preservation of nuclear identities in short evaporation cascades appear justified in the interpretation of the early observations [26] of regularities in the isotopic distributions of light and intermediate-mass clusters emitted in dissipative reactions close to the interaction barrier. As expected for equilibrium situations, the isotopic yields $Y_A(N_c,Z_c)$ of nuclear clusters (N_c,Z_c) resulting from the statistical decay of hot primary reaction products A were observed to track essentially with Boltzmann statistics,

$$Y_A(N_c,Z_c) \propto \exp\{-Q_{eff}^A(N_c,Z_c)/T\} \qquad (3)$$

involving the effective ground-state Q values, $Q_{eff}^A(N_c,Z_c)$, corrected for pairing and shell effects, for the emission of clusters from the emitter nucleus $A(N, Z)$ and the effective nuclear temperature T. In current terminology, such behavior is known as "iso-scaling," since the Q-values depend most strongly (quadratically) on the neutron-proton asymmetry or the nuclear isospin coordinates, $I = (N - Z)/2A$, of emitter and daughter nuclei. However, data obtained for the prevailing low nuclear excitations do not provide new information on the density dependence of the symmetry energy.

To produce nuclear systems at the subnormal densities of interest requires energetic reactions driving the nucleus toward complete disassembly. Here, the associated emission of pre-equilibrium particles, as well as the secondary statistical decay of highly excited nuclear clusters, complicates the interpretation of data. In order to eliminate some sensitivity of the data interpretation to associated systematic uncertainties, work reported [27-31] so far in the literature preferentially considers ratios of yields,

$$R_{12}(N_c,Z_c) = Y_2(N_c,Z_c)/Y_1(N_c,Z_c) \qquad (4)$$

of clusters (N_c, Z_c) emitted from different parent nuclei $i=1$,2. Since the binding energy of a nucleus depends approximately quadratically on neutron and proton numbers measured from the minimum of the valley of β stability, the individual yields are approximately Gaussians. Therefore, one expects a generally exponential dependence of the ratios of primary cluster yields,

$$R_{12}(N_c,Z_c) = \frac{Y_2(N_c,Z_c)}{Y_1(N_c,Z_c)} =: C\cdot\exp\{\alpha\cdot N_c + \beta\cdot Z_c\} \qquad (5)$$

Here, C is a constant, while the "isoscaling parameters" α and β reflect the ratios of the difference in curvatures of the β stable valley for the two emitters ($i=1,2$) and an effective temperature parameter T. For a thermodynamically equilibrated system, the latter parameter is identical to the equilibrium temperature given by the total available energy per nucleon in the system.

For an equilibrated system at constant temperature T, the following relations have been suggested [27, 28] between isoscaling parameters and symmetry energy coefficient C_{sym},

$$\beta = \frac{C_{sym}}{T}\cdot\Delta(N,A); \qquad \alpha = \frac{C_{sym}}{T}\cdot\Delta(Z,A) \qquad (6)$$

with the difference function Δ defined as

$$\Delta(X,A) = 4\cdot\left[\left(\frac{X}{A}\right)_1^2 - \left(\frac{X}{A}\right)_2^2\right] \quad (7)$$

influencing greatly the sensitivity of the isoscaling parameters to the symmetry energy.

In addition to the above ambiguity of the isoscaling parameters resulting already from an uncertain meaning of the effective temperature parameter, experimental uncertainties in the reconstruction of pre-evaporative cluster identities can further mask the relation between experimental isoscaling systematics and the symmetry energy of the highly excited emitters presumably at sub-normal densities.

This resolution effect is easily demonstrated for a generic stochastic isospin observable *Q (I)* and its probability distribution *P(Q)*. As an example, one can have *Q* represent the neutron number of an ensemble of clusters with a given Z-value (Z_c), rendering *P(Q)* the isotonic distribution for that element. In the present context, the first and (mostly) the second moments of the true probability distributions, $\langle Q\rangle$ and $\langle Q^2\rangle$, respectively, are of interest. However, the true probability distribution for the observable *Q* is not directly measurable but subject to finite experimental detection efficiency and resolution. Essentially, the true distribution *P(Q)* is folded with the experimental resolution function to yield the actually observed distribution *P'(Q)*. Approximately, the experimental resolution function can be represented by a Gaussian with second moment σ_ε^2. For poor resolutions, e.g. caused by significant neutron emission from the primary clusters, the observed distributions *P'(Q)* whose widths are essentially dominated by the width of the resolution functions. Taking the ratio of observed distributions $P_1'(Q)$ and $P_2'(Q)$ for two different emitting systems (*1* and *2*), as done typically in experimental analysis, amounts then to a comparison of two slightly displaced Gaussians. Under these conditions, one predicts a dependence of R_{12} on the observable *Q* to be given approximately by

$$\ell n\, R_{12} := \ell n\left[\frac{P_2'(Q)}{P_1'(Q)}\right] \approx \left[\frac{\Delta_{2-1}\langle Q\rangle^2}{2\sigma_\varepsilon^2}\right] + \left[\frac{\Delta_{2-1}\langle Q\rangle}{\sigma_\varepsilon^2}\right]\cdot Q \quad (8)$$

Here, the operator Δ_{2-1} denotes the difference of the corresponding quantity in system *2* minus that for system *1*. Obviously, in this approximation one expects a logarithmic straight line for the yield ratio $R_{12} = P_2'(Q)/P_1'(Q)$ when plotted vs. the observable *Q*, e.g., the neutron number for a fixed cluster element. However, in distinction to Equ. 5, the slope of the logarithmic line defined by Equ. 8 is determined by the difference in mean values of the two distributions and by the experimental resolution. Information on the desired second moments relating to the symmetry energy is no longer contained in this approximation. Both, slope and intercept of the isoscaling lines are strongly affected by the experimental resolution, and their valid interpretation relies therefore heavily on theoretical modeling, e.g., a good account of neutron evaporation processes.

B. Experimental Results and Discussion

The above obstacles limit the class of reactions that can provide reliable information on the symmetry energy of hot, expanded nuclear matter. Nevertheless, isoscaling analyses have been performed [26-34] for cluster emission in a variety of nuclear reactions, e.g., for dissipative collisions, multi-fragmentation at intermediate or relativistic energies and for statistical evaporation. The data discussed below emphasize the need for a reliable identification of the reaction mechanism as a prerequisite for a valid interpretation of the corresponding isoscaling data.

The present work reports on a new case of PLF cluster emission in dissipative reactions ^{48}Ca + ^{124}Sn and ^{48}Ca + ^{112}Sn at E_{lab}/A = *45 MeV*. As explained in Section III. In these experiments, kinematically well identified Ca-like PLFs from dissipative interactions of Ca projectile ions with with Sn target nuclei are observed to split in a fission-type fashion into an intermediate-mass cluster and a PLF remnant. It is known from the multiplicities of associated light charged particles that these events emerge from a range of impact parameters intermediate between peripheral and central collisions.

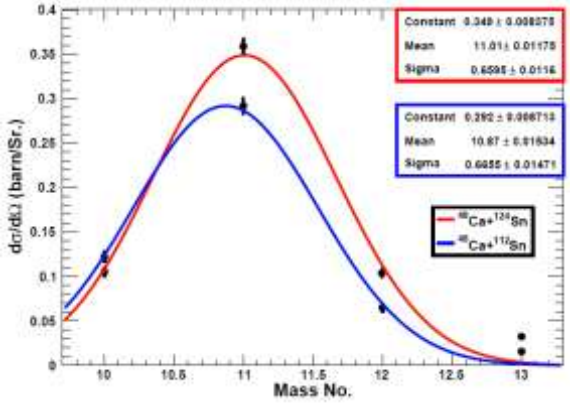

Figure 6: Angle-integrated isotopic distributions of B clusters emitted in splits of PLFs from reactions induced by ^{48}Ca on ^{112}Sn and ^{124}Sn targets. The curves represent Gaussian fits.

As an example of the quality of data obtained in the present experiment, Fig. 6 exhibits angle-integrated isotopic yields for *B* clusters emitted in the dynamical breakup of *PLF*s from the two reactions. The smooth curves represent Gaussian fits used here just to guide the eye, while the quantitative analysis of isotopic ratios discussed below relies on an integration of the measured data.

From the data displayed in Fig. 6 one observes higher yields of the heavier B isotopes from PLFs emerging from reactions with the more neutron rich ^{124}Sn target. Conversely, lighter isotopes are produced with greater probabilities from splits of PLFs after a reaction with the lighter ^{112}Sn target nucleus. The corresponding relative enhancements are characteristic not only for the integrated yields but persist consistently over the range of forward angles ($6^o \le \theta \le 20^o$).

In the following discussion, the integrated measured yields of given cluster isotopes (*N, Z)* from the breakup $PLF^* \rightarrow PLF' + (N,Z)$ are plotted as ratios from the two

reactions vs. cluster neutron or proton number (*N* or Z) in the form

$$Ratio(N,Z) = Y_{N,Z}\left({}^{48}Ca + {}^{124}Sn\right) \Big/ Y_{N,Z}\left({}^{48}Ca + {}^{112}Sn\right) \quad (9)$$

At this stage, no evaporation or other corrections aimed at a reconstruction of the primary *PLF** have yet been applied to these data. It is also noted that no angular restriction has been applied to the data with respect to the alignment of the breakup axis within the experimentally well-defined reaction plane.

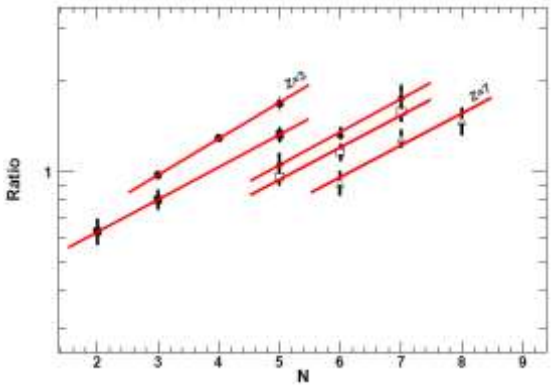

Figure 7: Isoscaling plot for Li, Be, B, C, and N clusters from breakup of PLFs from dissipative ^{48}Ca+^{124,112}Sn collisions at E/A=45 MeV.

Data for the measured raw isotopic ratios for *Li*, *Be*, *B*, C and *N* clusters are shown in Fig. 7 on a semi-logarithmic scale vs. cluster neutron number *N*. No evaporation or other corrections aiming at a reconstruction of the pre-evaporative PLF have been applied. Yet, the plot obviously demonstrates the familiar phenomenon of isoscaling. This is in contrast to some of the earlier studies of the effect for projectile fragmentation [32, 33] where such isoscaling was not observed without prior approximate reconstruction of the primary projectile-like fragment *PLF** and then only for isotopic data sorted according to different bins in *N/Z* value of the reconstructed fragment *PLF**.

It is shown in Fig. 7 for the clusters emitted in *PLF** breakup for present Ca+Sn reactions, the raw experimental yield ratios for all isotopes of a given element fall on a semi-logarithmic straight line, and the lines for different elements are parallel to one another. Going from one element to the next heavier element for a given *N*, the isotopic ratios are seen to decrease by an approximately constant factor, except for the change from *Z* = 5 to *Z* = 6. A corresponding behavior is observed for isotone ratios plotted vs. cluster *Z*-value.

As a further step in the data reduction, "global" isoscaling parameters $\bar{\alpha}$ and $\bar{\beta}$ were derived from a combination of all isotope or isotone data, respectively. For this purpose the data are plotted in one of the two forms,

$$\begin{aligned} S(N) &:= R_{12}(N,Z)\cdot\exp\{-\beta\cdot Z\} \approx C\cdot\exp\{\bar{\alpha}\cdot N\} \\ P(Z) &:= R_{12}(N,Z)\cdot\exp\{-\alpha\cdot N\} \approx C'\cdot\exp\{\bar{\beta}\cdot Z\} \end{aligned} \quad (10)$$

The approximate equalities in this equation refer to the expectation that such plots, *S*(*N*) or *P*(*Z*), would show systematic trends in the individual isoscaling parameters defined by the *r.h.s.* of Equ. 10 with mean values $(\bar{\alpha}, \bar{\beta})$.

As an example, individual values for $S(N)$ defined on the *l.h.s.* of Equ. 10 are plotted in Fig. 8 vs. cluster neutron number *N*, for the same elements. Also shown in this figure is a semi-logarithmic fit line defining an average value of $\bar{\alpha} = (0.23 \pm 0.02)$ for the set of individual isoscaling parameters α, as defined in Equ. 10. This line appears to fit very well the individual values which show no systematic deviation from the fit. A similar procedure was applied to deduce a mean isoscaling parameter $\bar{\beta}$ from fitting a logarithmic straight line to individual functional values $P(Z)$. This procedure produced a global isoscaling parameter of $\bar{\beta} = (-0.12 \pm 0.01)$.

The magnitudes of the above mean ("global") isoscaling parameters obtained from these fits are significantly smaller, by factors of 3 to 4, than reported in other works [27-34]. The latter experiments have studied projectile fragmentation, albeit for projectiles heavier than calcium. Because of these observational discrepancies, care was taken in the present work to investigate the sensitivity of the data analysis to the applied sorting criteria. Specifically, the sensitivity of the results was investigated for two important criteria, constraints imposed on the relative velocity v_{rel} between the IMF cluster and projectile remnant and on the accepted degree of alignment of the PLF* breakup axis within the reaction plane.

The relative velocity v_{rel} between the IMF cluster and

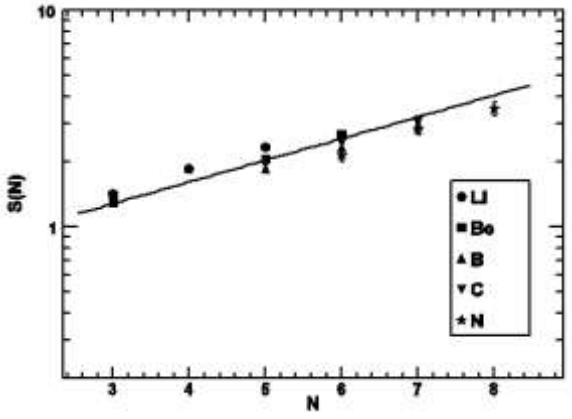

Figure 8: Global isoscaling function *S(N)* vs. neutron number. The logarithmic straight line represents a best fit to individual data.

projectile remnant is important in suppressing potential contamination of the data set by particles emitted from the target-like fragment. In the sensitivity test, the accepted range of velocities was changed from its normal range ($1.0 \le v_{rel}/v_c \le 2.0$), to include events with larger relative velocities, $v_{rel}/v_c > 2.0$. Here, v_c is the reference velocity due to Coulomb repulsion of spherical fragments. It turned out that such a modification to the analysis had little effect on the results, the modified calculation yielded

global isoscaling parameters well within the quoted uncertainties for $\bar{\alpha}$ and $\bar{\beta}$.

Changes in the restrictions imposed on the out-of-plane angular (ϕ) orientation of the breakup axis accepted for analysis ($\cos(\varphi) \leq 0.4$) turned out to be similarly inconsequential for the values deduced for the pair of global isoscaling parameters $\bar{\alpha}$ and $\bar{\beta}$ fitting the isotopic systematics very well. Again, the variations of these parameters obtained with a relaxed angular constraint are inside the quoted uncertainties. The global isoscaling parameters quoted above must therefore be considered robust results of the present experiments. The smaller isoscaling parameters deduced in the present experiments are therefore likely due to greater similarities in *A/Z* between the PLF* emitters, i.e., smaller values of the difference functions Δ.

A further, detailed interpretation of the observed isotopic regularities requires knowledge of the identities and physical properties of the PLF* nuclei producing the cluster distributions discussed here, along with the effects of secondary decays of the primaries. Equations 6 and 7 display relations between isoscaling parameters, the *A/Z* ratios of the cluster emitters and the symmetry energy, for a system at thermodynamic equilibrium characterized by a temperature *T*. Essentially, either isoscaling parameter is given by the difference in the ratios of the energies required to produce a cluster of given A/Z and the specific energy available per degree of freedom.

Lacking detailed experimental knowledge of the emitter identities in the present ^{48}Ca+^{112,124}Sn reactions, a less direct strategy is adopted in this work by searching for an initial hypothetical picture that evolves plausibly into a final scenario which agrees well with the important experimental phenomena. Here, one searches for the difference $\Delta B = B_2 - B_1$ in energy cost for a given cluster to be emitted from either PLF* in a binary split and the effective energy T_{eff} available for such emission process. Because of the similarity of the two systems and bombarding energies, the effective temperature can be assumed to be similar for the corresponding PLF* cluster emitters, i.e., $T_{eff,1} \approx T_{eff,2} = T_{eff}$. Cluster energy spectra, which were also measured in the present experiments, suggest a range of $3MeV \leq T_{eff} \leq 4MeV$ for possible values of the effective temperature.

In the above picture, cluster yield ratios would be parameterized as

$$R_{21}(N,Z) = Y_{N,Z}\left({}^{48}Ca + {}^{124}Sn\right) \Big/ Y_{N,Z}\left({}^{48}Ca + {}^{112}Sn\right) = \exp\{\frac{\left[B_2(N,Z) - B_1(N,Z)\right]}{T_{eff}}\} = \exp\{\frac{\Delta B}{T_{eff}}\} \quad (11)$$

Here, the quantity ΔB represents the difference in binding energies of a given IMF cluster in the primary neutron rich and neutron poor PLF*, respectively. A search was made for the Z and A values of the two possible PLF* emitter nuclei, whose binding energy differences for break-up into different IMFs would follow the experimental yield ratios R_{12}(N,Z). It is obvious from Equ. 11 that this type of analysis determines only ratios of $\Delta B / T_{eff}$ consistent with the data such that more than one set of variables (Z_1, Z_2, A_1, A_2, T_{eff}) can describe the two decaying projectile-like fragments *PLF** and lead to similar isoscaling behavior. Additional information is required, based on other reaction characteristics, to constrain the potential continuum of possible solutions.

An example of such an analysis is depicted in Fig. 9, where experimental yield ratios are plotted on a semi-logarithmic scale vs. cluster binding energy differences ΔB calculated for breakup of *PLF** nuclei with $PLF_1^* = (Z_1 = 20, A_1 = 49)$ and $PLF_2^* = (Z_2 = 18, A_2 = 43)$. The line drawn through the data in Fig. 9 corresponds to an effective temperature parameter of $T = (2.6 \pm 0.3)$ *MeV*. A second representation of the data of similar quality can be obtained with Equ. 11, assuming *PLF** breakup of $PLF_1^* = (Z_1 = 25, A_1 = 48)$ and $PLF_2^* = (Z_2 = 26, A_2 = 49)$. In this case, the logarithmic straight line representing the experimental yield ratios corresponds to a high effective temperature parameter of $T = (5.5 \pm 0.3)$ MeV.

Of the two sets of fit results identifying possible candidates for primary projectile-like fragments undergoing inelastic breakup following a dissipative reaction, the first represents the more likely scenario. Here the mean

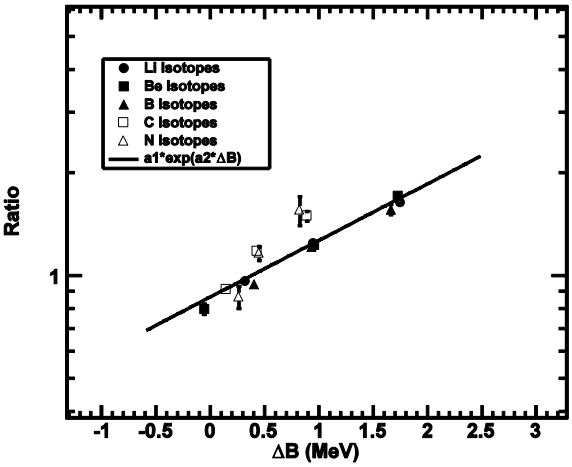

Figure 9: Scaling of experimental cluster yield ratios for ^{48}Ca + ^{124,112}Sn reactions at E/A=45 MeV based on ground-sate binding energy differences (cf. Equ. 11).

changes in atomic and mass numbers of the PLF* relative to the projectile are relatively small. Such behavior is consistent with the liquid-drop potential energy surfaces driving nucleon exchange in dissipative reactions. It is also consistent with the similar ^{40,48}Ca+^{112}Sn reactions measured at *E/A=35 MeV* [6]. In contrast, the second set of parameters corresponds to highly unlikely proton pickup by the projectile and very high temperatures which neither IMF nor heavier PLF* remnants could survive intact.

In view of the stark discrepancy pointed out earlier between the experimental values for isoscaling parameters derived in the present work and values reported in the literature, it is interesting to explore whether the present reaction is an exception also as far as the scaling of isotopic yields with ground state binding energies (cf. Fig. 9) is concerned. Therefore, a similar analysis was carried out

for the isoscaling data reported [32], for the decay of partially reconstructed projectile-like fragments emitted in the pair of reactions ^{86}Kr + ^{64}Ni and ^{78}Kr + ^{58}Ni reactions at *E/A=35 MeV*.

For the above reactions, isotopic distributions have been measured for a broad range of IMF clusters with atomic numbers Z = 3-17. For these data, isoscaling was not observed for the raw data but appeared for the reconstructed *PLF**. A search was conducted for a set of primary projectile-like fragments from these reactions, whose ground state binding energy patterns represent experimental yield ratios in a functional form given by Equ. 11and acceptable, plausible parameters for the effective temperature parameter T_{eff}.

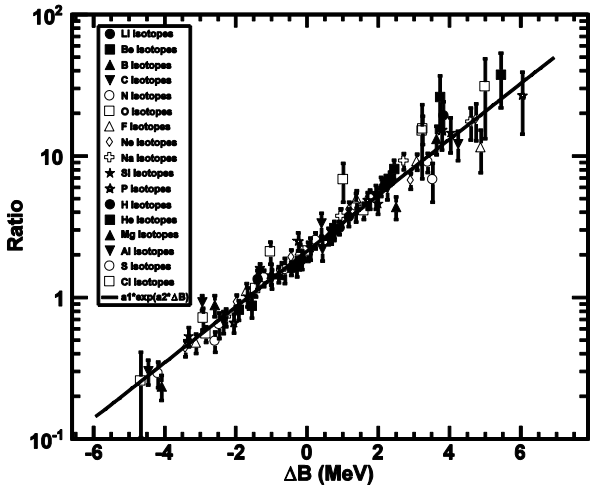

Figure 10: Scaling of experimental yield ratios with binding energy differences for ^{86,78}Kr + ^{64,58}Ni reactions at E/A=35 MeV. Data imported from [32].

In fact, that search was successful and has identified a set of *PLF** candidates $PLF_1^* = (Z_1 = 40, A_1 = 89)$ and $PLF_2^* = (Z_2 = 39, A_2 = 84)$ fitting the data with Equ. 11, using the corresponding ground-state binding energies. An effective temperature of $T = (2.2 \pm 0.2)$ *MeV* was derived from the fit, which is shown in Fig 10, together with the data from the present experiment. Obviously, this figure demonstrates a remarkable agreement of a large data set with the ground-state binding-energy systematics defined by Equ. 11. In addition, the effective temperature parameter deduced for the *Kr+Ni* data is very similar to the results reported for the present *Ca+Sn* reactions, in spite of the different bombarding energies. This implies that these very different experiments produce isotopic yield of *PLF* clusters that fit universal systematics based on ground state *Q* values for cluster emission.

V. CONCLUSIONS

In summary, experimental data are presented for a dynamical breakup process of a fairly light projectile (Ca) following a dissipative primary reaction. Memory contained in a strongly aligned breakup axis suggests proximity interactions with the target nucleus during the breakup process. Calculations with several reaction models did not succeed in reproducing experimental observations. *Ad hoc* phase space models of breakup proposed in the literature are employed to provide an approximate framework for an interpretation of the breakup data.

In the experiments, the breakup of the projectile-like fragment (*PLF**) is seen to produce intermediate-mass clusters and heavier remnants which exhibit isotopic regularities known as isoscaling. The isoscaling parameters deduced from fits of isotopic cluster distributions are robust; their values do not show appreciable dependencies on variations in the analytical procedures. Although the deduced parameter sets are not unique, additional knowledge about the primary reaction is useful in constraining the associated ambiguity.

New global systematics of isotopic cluster distributions was found to apply equally to several different reaction pairs. The associated isoscaling appears to be governed by ground-state *Q* values based on the masses of nuclei at normal densities. It does not appear to give direct and unambiguous access to the symmetry energy at subnormal matter densities. Better success to achieve this goal may require studies of simpler composite systems produced closer to equilibrium.

ACKNOWLEDGMENTS

This work was supported by the US Department of Energy Grant No. DE-FG02-88ER40414. The authors express their gratitude to the LNS CS operational crew for providing excellent beams. The non-resident authors like to thank their LNS colleagues and the LNS staff for the hospitality and support extended to them.

REFERENCES

1. J. Richert and P. Wagner, Phys. Reports C 350, 1 (2001) and references.
2. A. Bonasera et al., Rev. Nuovo Cim. 23, 1 (2000).
3. Ph. Chomaz, M. Colonna and J. Randrup, Phys. Reports 389, 263 (2004) an references.
4. J. Tõke, J. Lu and W.U. Schröder, Phys. Rev. C 67, 034609 (2003).
5. J. Tõke and W. U. Schröder, Phys. Rev. Letters 82, 5008 (1999).
6. B.A. Li and W. U. Schröder (Editors), *Isospin Physics in Heavy-Ion Collisions at Intermediate Energies*, Nova Science Publ., Inc., Huntington, New York, 2001.
7. W. U. Schröder and R. J. Huizenga, Treatise on Heavy Ion Science, edited by D. A. Bromley (Plenum Press, New York, 1984).
8. J. P. Blaizot, Phys. Reports 64, 171 (1980)
9. B. A. Li, L.W. Chen, C. M. Ko, Phys. Reports 464, 113 (2008); and references.
10. M. Blann, Annu. Rev. Nucl. Sci. 25, 123 (1975)
11. E. Gadioli and P.E. Hodgson, Pre-Equilibrium Nuclear Reactions, Clarendon Press, Oxford (1992).
12. W. U. Schröder and J. Tõke, Nucl. Phys. A681, 418c (2001).
13. M. A. Famiano et al., Phys.Rev Letters 97, 052701 (2006).

14. N. L. Neindre et al., Nucl. Instrum. Methods. Phys. Res. A, 490, 251 (2002).
15. M. Alderighi et al., Nucl. Instrum. Methods. Phys. Res. A, 489, 257 (2002).
16. A. Pagano et al., Nucl. Phys. A., 734, 504 (2004).
17. M. J. Quinlan, PhD Thesis, University of Rochester, 2011, and to be published.
18. W.U. Schröder et al., *Proc. Int. Symp. Nucl. Fission and Heavy-Ion-Induced Reactions,Harwood Academic Press, New York, Nucl. Sci. Res. Conf. Ser. Vol. 11*, 255 (1987).
19. R. J. Charity et al., Nucl. Phys. A., 483, 371 (1988).
20. J. Lukaczik and Z. Majka, Acta Phys. Pol. 24, 1959 (1993).
21. H. Fuchs and K. Möhring, Rep. Prog. Phys. 57, 231 (1994)
22. P. Glaessel et al., PRL 48, 1089 (1982).
23. I. Halpern, Annu. Rev. Nucl. Sci. 21, 245 (1971)
24. J. P. Lestone, Phys. Rev. C 70, 021601(R) (2004)
25. V. A. Rubchenya et al., Proc. Workshop Nucl. Fission and Fission Product Spectr., ILL Report 94FA05T, 26 (1994).
26. V.V. Volkov, Phys. Rep. 44, 93(1978); and references.
27. [9] M. B. Tsang et al., Phys. Rev. Lett., 86, 5023 (2001).
28. [16] A. S. Botvina et al., Phys. Rev. C., 65, 044610 (2002).
29. [18] J. Brzychczyk et al., Phys. Rev. C., 47, 1553 (1993).
30. [19] Z. Chen et al., Phys. Rev. C., 81, 064613 (2010).
31. A.B. McIntosh et al., Phys. Rev. C 81, 034603 (2010).
32. S. Wuenschel et al., Phys. Rev. C., 79, 061602(R) (2009).
33. S. Galanopoulos et al., Nucl. Phys. A., 837, 145 (2010).
34. D. V. Shetty et al., Phys. Rev. C., 71, 024602 (2005).

.